

General Disclaimer

One or more of the Following Statements may affect this Document

- This document has been reproduced from the best copy furnished by the organizational source. It is being released in the interest of making available as much information as possible.
- This document may contain data, which exceeds the sheet parameters. It was furnished in this condition by the organizational source and is the best copy available.
- This document may contain tone-on-tone or color graphs, charts and/or pictures, which have been reproduced in black and white.
- This document is paginated as submitted by the original source.
- Portions of this document are not fully legible due to the historical nature of some of the material. However, it is the best reproduction available from the original submission.

Cross Spectra Between Pressure and Temperature in a Constant-Area Duct Downstream of a Hydrogen-Fueled Combustor



J. H. Miles, C. A. Wasserbauer,
and E. A. Krejsa
*Lewis Research Center
Cleveland, Ohio*

(NASA-TM-83463) CROSS SPECTRA BETWEEN
PRESSURE AND TEMPERATURE IN A CONSTANT-AREA
DUCT DOWNSTREAM OF A HYDROGEN-FUELED
COMBUSTOR (NASA) 30 p HC A03/MF A01

N84-11885

Unclass

CSCI 20A G3/71 42456

Prepared for the
One-hundred-fifth Meeting of the Acoustical Society of America
Cincinnati, Ohio, May 10-13, 1983

NASA

CROSS SPECTRA BETWEEN PRESSURE AND TEMPERATURE
IN A CONSTANT-AREA DUCT DOWNSTREAM OF A
HYDROGEN-FUELED COMBUSTOR

J. H. Miles, C. A. Wasserbauer, and E. A. Krejsa
National Aeronautics and Space Administration
Lewis Research Center
Cleveland, Ohio 44135

ABSTRACT

Pressure-temperature cross spectra are necessary in predicting noise propagation in regions of velocity gradients downstream of combustors if the effect of convective entropy disturbances is included. In the present study pressure-temperature cross spectra and coherences were measured at spatially separated points in a combustion rig fueled with hydrogen. Temperature-temperature and pressure-pressure cross spectra and coherences between the spatially separated points as well as temperature and pressure autospectra were measured. These test results were compared with previous results obtained in the same combustion rig using Jet A fuel in order to investigate their dependence on the type of combustion process. The measurement technique used a dual-thermocouple probe and an "infinite" tube microphone. The measurements were made near the inlet and exit of a 6.44-m-long duct attached to a J-47 combustor. As with the Jet A tests some combustion occurred in the long duct. The test results for both fuels were similar. For example, at the duct exit for several 10-Hz segments the phase angle between the pressure and the temperature was a linear function of frequency with a slope proportional to the convective time delay. This is similar to the behavior found for tests done in the same rig using Jet A fuel. However, the significant coherence at low frequencies between the pressure and temperature at the duct exit observed in the Jet A data was not present. Also, as with the Jet A data definite phase relationships of unknown origin between pressure and temperature were observed in the pressure-temperature cross spectra at the duct inlet. This indicates a systematic relationship. These phase relationships are not consistent with a simple source model that assumes that pressure and temperature are in phase at a point in the combustor and at all other points downstream are related to one another by only a time delay due to convection of temperature disturbances. Thus these test results indicate that a more complex model of the source is required.

E-1779

SYMBOLS

A	thermocouple parameter
d	wire diameter
f	frequency
Δf	frequency interval
G_{ij}	thermocouple autospectrum
G_{ij}	thermocouple cross spectrum
H_{ij}	ratio of thermocouple autospectrum to cross spectrum, G_{ij}/G_{ij}

<i>Im</i>	imaginary part
<i>i</i>	$\sqrt{-1}$
<i>L</i>	distance between points
<i>P</i>	penalty function
<i>p</i>	acoustic pressure
<i>Re</i>	real part
<i>S</i>	quadratic error function
<i>T</i>	temperature perturbation
<i>t</i>	time
<i>W_{air}</i>	air mass flow rate
<i>V</i>	mean flow velocity
<i>u, v, w</i>	weighting factors
<i>Y</i>	thermocouple output voltage
$\Delta\theta$	phase shift
<i>n</i>	temperature-voltage conversion constant
τ	time constant
ω	angular frequency, $2\pi f$

Superscript:

(*)** complex conjugate

Subscripts:

b bead
g gas
i arbitrary index
m measured
max maximum
w wire
1,2 thermocouples
3,4 duct locations
∞ far from bead

INTRODUCTION

Describing noise propagation in a variable-velocity region downstream of a combustor in a turbofan engine requires that both the temperature autospectrum and the pressure-temperature cross spectrum at the combustor inlet be specified to account for the effect of convective entropy disturbances (ref. 1). In reference 1 it is hypothesized that a nonrandom relationship

exists between pressure and temperature disturbances downstream of a combustor and that the phase relationship between pressure and temperature is due to the convective time delay. A literature search revealed that, although measurements of pressure and temperature autospectra in combustion systems have been made (refs. 2 to 5), measurements of the cross spectra between temperature and pressure were not available. Consequently, as part of a program to investigate turbofan engine core noise conducted at the NASA Lewis Research Center, a technique was developed to measure temperature-pressure cross spectra in a combustion rig over the range of frequencies of interest in combustion noise studies (ref. 6).

This technique was applied to a combustion system consisting of a J-47 can combustor followed by a 6.44-m-long duct. The results obtained using liquid Jet A fuel were presented in reference 6. The technique uses a dual (thick and thin) Chromel-Alumel thermocouple probe to measure temperature and an "infinite" tube microphone to measure pressure. The technique has the limitation that the sensitivity of the thermocouple is reduced as the frequency is increased because the thermocouple response is approximately that of a first-order lag system. Thus above 30 Hz the temperature-temperature cross spectra presented in reference 6 were contaminated by noise. However, the pressure-temperature cross spectral noise floor was not reached until at least 100 Hz.

The results in reference 6 are for cases where some combustion was occurring in the duct. Below 30 Hz the temperature cross spectra between the inlet and the exit showed that temperature perturbations at the inlet and exit of the long duct were related by the convective time delay. Also, at the duct inlet and exit the magnitudes of the cross spectra between pressure and temperature resembled the magnitude of the corresponding pressure autospectrum. At the duct inlet the phase angle between the pressure and the temperature had some evidence of distinct patterns indicating a systematic relationship. No clear relationship to the pattern that would be produced by a convective time delay was observed. However, at the duct exit the phase angle between the pressure and temperature below 100 Hz had a linear dependence with slopes proportional to the time delay due to convection of temperature disturbance in the long duct. An extrapolation of the cross spectra phase angles suggested that a localized region in the combustor exists such that the acoustic pressure and temperature perturbations are not greatly out of phase at low frequencies. This localized region is defined as the source point based on a simple model for the source region that assumes that pressure and temperature are in phase at the source point in the combustor and related to one another by only a time delay due to convection of temperature disturbances at all other points.

Having developed a pressure-temperature cross spectral measurement technique and having obtained some baseline data, questions immediately arose about how general the results were and how much they depended on the combustion process. Consequently this study was conducted to obtain data with gaseous fuel (hydrogen) instead of liquid fuel (Jet A) in the identical combustion system.

The thermocouple calibration procedure discussed in reference 6 was based on a single-parameter model and required finding a single time constant for each of the wires in the dual probe. For the temperature data reported in this paper a more general calibration procedure was applied. The procedure

was based on a three-parameter model that includes, in addition to heat transfer from the gas to the thermocouple, the heat transfer from both the gas and the wire to a bead at the junction of the two wires in each thermocouple. If the bead size equals the wire size, both models produce a similar correction.

This paper presents measurements of pressure-temperature cross spectra and coherence and pressure and temperature autospectra near the inlet and exit of a long duct downstream of a hydrogen-fueled combustor. In addition, pressure and temperature cross spectra and coherence between the inlet and exit of the long duct are shown. For the case presented, some combustion occurred in the long duct.

TEST FACILITY, INSTRUMENTATION, AND THERMOCOUPLE CALIBRATION

The temperature and pressure measurements were made in the combustion rig shown in figure 1, which consisted of a J-47 can combustor (fig. 1(b)) mounted in a 0.203-m-diameter by 0.77-m-long test section and an attached 6.44-m-long by 0.203-m-diameter stainless steel duct. The fuel used was hydrogen. Pressure and temperature measurements at stations 3 and 4 are discussed. All tests were conducted at the outdoor acoustic arena shown in figure 2.

Tests were run at mass flow rates of 0.5 and 1.1 kg/s with nominal inlet temperatures of 830 and 1200 K. Only the higher-flow-rate test condition at the lower temperature is presented because, for the comparisons made using the pressure-temperature and temperature-temperature cross spectra and coherences, these results are typical. However, significant differences were observed in the pressure and temperature autospectra at the two flow rates because of stronger coupling between the combustion process and a longitudinal acoustic mode at the lower mass flow rate. The coupling at the lower flow rate was strong enough to cause a peak to occur in the temperature autospectrum at a frequency corresponding to a tone in the pressure autospectrum. The pressure and temperature autospectra at the higher flow rate resemble those observed for the Jet A tests reported in reference 6.

The conditions for the test point discussed herein are given in table I. Note that the duct exit temperature was higher than the inlet temperature, indicating combustion occurred in the duct as it did in reference 6.

Pressure Measurements

The internal pressure transducers used were conventional 0.635-cm microphones with pressure response cartridges. To avoid direct exposure of the microphone to the combustion gases, they were mounted outside the ducted combustion rig, and the fluctuating pressure in the rig was transmitted to the transducers by means of a "semi-infinite" acoustic waveguide. Details of these probes are given in references 7 and 8.

Temperature Measurements

The temperature fluctuations were measured with Chromel-Alumel thermocouples. The dual-thermocouple probe design shown in figure 3 was selected so that the response time of the thermocouple could be determined from the actual

test data rather than from a separate precalibration. A calibration procedure based on the procedure discussed in reference 9 was used. The thermocouple wire diameters were 76.2 and 25.4 μm . Examination of one of the dual-probe thermocouples showed that the diameter of the bead on the thin thermocouple was about three times the diameter of the thin thermocouple wire while the bead on the thick thermocouple was about twice the diameter of the thick wire. The thermocouples were inserted into the duct by actuators after combustion started in order to prevent their destruction by the combustion startup transient.

Data Acquisition and Processing

Signals from the pressure and thermocouple probes were simultaneously recorded on magnetic tape for later processing. Signals were recorded for 2 minutes at each operating condition. The microphones were calibrated each day with a standard pistonphone before data were recorded. The thermocouples were used simultaneously to measure mean temperature. The signal cross and auto-spectra were obtained by off-line processing of the tape-recorded data on a two-channel fast-Fourier-transform digital signal processor with built-in analog-to-digital converters and 120-dB/octave antialiasing filters. The resulting spectra were then transmitted from the processor to a central computer. The central computer was used to analyze the thermocouple data so that the thermocouple could be calibrated. The calibration correction was incorporated in a central computer program used to plot the data.

Thermocouple Calibration

The approach used to calibrate the thermocouple was based on the dual-thermocouple method described in reference 9. However, in reference 9 the thermocouple model used the ideal thermocouple geometry of an infinitely long wire of constant diameter with no bead at the junction of the wires. For this model the gas temperature T_g and the bead junction temperature T_b are related by

$$T_g = T_b + \tau_w \left(\frac{\partial T_b}{\partial t} \right) \quad (1)$$

where τ_w is the thermal time constant of an infinite wire.

In this study the "bead" formed by joining the wires was taken into account by using a thermocouple model discussed in reference 10. The "bead" energy conservation equation derived in reference 10 is

$$T_g = T_b + \tau_b \left(\frac{\partial T_b}{\partial t} \right) - A(T_{w\infty} - T_b) \quad (2)$$

and for the wire far from both the bead and the supports

$$T_g = T_{w\infty} + \tau_w \left(\frac{\partial T_{w\infty}}{\partial t} \right) \quad (3)$$

where A approximates the ratio of the bead-to-wire heat transfer coefficient to the gas-to-bead heat transfer coefficient, T_b is the time constant for direct heat exchange between the bead and the gas, and T_w is the wire temperature far from the bead and supports.

Combining the Fourier transform of equations (2) and (3) to find the relationship between the bead temperature T_b and the gas temperature T_g yields

$$T_g(i\omega) = T_b(i\omega) \frac{(1 + A + i\omega\tau_b)(1 + i\omega\tau_w)}{(1 + A + i\omega\tau_w)} \quad (4)$$

For a bead diameter very nearly the same as the wire diameter, A is greater than unity and equation (4) resembles the Fourier transform of equation (1). For a bead diameter larger than the wire diameter, heat transfer from bead to wire is dominated by convection from gas to bead so that A is nearly zero and only the bead time constant is important.

In the method discussed in reference 9 thick and thin wire thermocouples, denoted 1 and 2, are placed in the flow near one another so as to experience the same temperature-time history. The fluctuating thermocouple voltage Y is proportional to the bead junction temperature T_b . Thus the Fourier transform of the voltage signal is given by

$$Y(i\omega) = n \frac{T_g(i\omega) (1 + A + i\omega\tau_w)}{(1 + i\omega\tau_w) (1 + A + i\omega\tau_b)} \quad (5)$$

The autospectra of the thick and thin wire thermocouples are given by

$$G_{11} = Y_1 Y_1^* \quad (6)$$

$$G_{22} = Y_2 Y_2^* \quad (7)$$

and the cross sp

$$G_{12} = Y_1 Y_2^* \quad (8)$$

Constructing the ratios

$$H_{11} = \frac{G_{11}}{G_{12}} \quad (9)$$

and

$$H_{22} = \frac{G_{22}}{G_{12}} \quad (10)$$

produces functions that depend on only the thermocouple model parameters because the relationship between bead temperature and voltage is the same for both thermocouples and because the thermocouples are close enough together to be subjected to the same temperature-time history.

For the thermocouple model used in reference 9, based on equation (1), the time constants could be estimated from examination of the real and imaginary values of H_{ij} calculated from the data since for this model $\text{Im}(H_{ij})$ has a maximum at $1/\tau_j$ and

$$\lim_{\omega \rightarrow \infty} H_{11} = \frac{\tau_2}{\tau_1} \quad (11)$$

and

$$\lim_{\omega \rightarrow \infty} H_{22} = \frac{\tau_1}{\tau_2} \quad (12)$$

Another characteristic of this model is that the time constant for an infinite wire thermocouple is roughly proportional to $d^{1.5}$, where d is the wire diameter. In reference 9, 76.2- and 25.4- μm -thick wires were used, and it was found that the ratio of time constants was roughly $3^{1.5} = 5.2$. In reference 6 the ratio of time constants varied from 1.7 to 2.3. Furthermore the theoretical H_{ij} function based on equation (1) and used in reference 6 to fit the measured H_{ij} function did not fit at all points. Because of the deviations found in reference 6 from results obtained using the infinite wire model and because of the observed large beads at the thermocouple junction, the new model described by equations (2) and (3) is used herein.

For the more complex thermocouple model a nonlinear programming technique was used to find the constants that minimized a nonlinear quadratic performance measure S . The value of S is equal to the weighted least-squares error between the measured and theoretical values of H_{11} and H_{22} plus a penalty function used to constrain the values of the constants. Thus

$$S = \sum_{i=1}^2 \left\{ w_i \left[\text{Re}(H_{ij})_m - \text{Re}(H_{ij}) \right]^2 + v_i \left[\text{Im}(H_{ij})_m - \text{Im}(H_{ij}) \right]^2 + P \right\} \quad (13)$$

and

$$P = \sum_{i=1}^2 \left\{ u_{1i} \left[\tau_w(i) - \tau_{w,\max} \right]^2 + u_{2i} \left[\tau_b(i) - \tau_{b,\max} \right]^2 + u_{3i} \left[A(i) - A_{\max} \right]^2 \right\} \quad (14)$$

where

$$u_{1i} = \begin{cases} 0 & \tau_w(i) < \tau_{w,max} \\ 1 & \text{otherwise} \end{cases}$$

$$u_{2i} = \begin{cases} 0 & \tau_b(i) < \tau_{b,max} \\ 1 & \text{otherwise} \end{cases}$$

$$u_{3i} = \begin{cases} 0 & A(i) < A_{max} \\ 1 & \text{otherwise} \end{cases}$$

The conjugate-direction search technique used to minimize S in this study is described in reference 11, and the computer program used was adapted from reference 12. The model parameters in all cases were determined by using the spectrum between 0 and 32 Hz because in this region the temperature cross spectra change significantly. Once determined, these parameters are valid at all higher frequencies where the model described by equations (2) and (3) is valid.

In order to demonstrate the procedure, typical constant-bandwidth (0.08 Hz) dual-thermocouple cross spectra and autospectra measurements before and after correction for the time constants determined by the search technique are shown in figures 4 and 5. The corresponding coherence function is shown in figure 6. Note that the thermocouple coherence is near unity (fig. 6). This is a necessary condition for application of the calibration procedure since it means that extraneous noise is low and that the thermocouples experience essentially the same temperature-time history. The measured values of H_{11} and H_{22} are shown in figures 7 and 8 in terms of their real and imaginary components along with the least-squares curve fits used to find the time constants. Table I gives the constants used to correct the case described herein.

The coherences between the thick and thin thermocouples at the duct inlet and exit are shown in figures 9 and 10 for the frequency range from 0 to 320 Hz. The inlet coherence is near unity over the whole frequency range, but the exit coherence is near unity only below 40 Hz. This does not invalidate the calibration at the exit since the thermocouple constants are defined by the behavior of the thermocouples below 30 Hz. However, it did make it necessary to compare the signals from the thick and thin thermocouples and their respective pressure-temperature cross spectra. It was found that at the high flow rate the thick-thermocouple signal had less noise and produced a better pressure-temperature cross spectrum. Consequently for the exit test point, only pressure-temperature cross spectra obtained using the thick thermocouple are presented.

RESULTS

This section discusses measurements of pressure-pressure and temperature-temperature cross spectra between the inlet and exit of the long duct. Also, pressure-temperature cross spectra at the duct inlet and exit are discussed. Only one test condition as defined in table I is shown.

With each cross spectrum the corresponding coherence function is presented. Note that a coherence smaller than unity implies that one or more of the following conditions exists:

- (1) Extraneous noise is present in the measurements.
- (2) The system relating the output to the input is nonlinear.
- (3) The output is due to more than one input.

Pressure Cross Spectra, Autospectra, and Coherence

The constant-bandwidth (0.8 Hz) pressure-pressure cross spectrum between the duct inlet and the exit is shown in figure 11 and pressure autospectra at the duct inlet and exit are shown in figure 12. The cross spectra and autospectra magnitude plots show cancellations and reinforcements due to the longitudinal standing wave pattern. The rolloff at low frequencies shown in the duct exit autospectra is due to the impedance at the exit. The cross spectral phase shifts of 180° are also due to the longitudinal standing wave in the duct. The linear overall increase in phase angle is due to the flow effect on acoustic propagation in the duct.

The corresponding coherence function is shown in figure 13. The coherence is essentially unity except at frequencies where the signal goes to zero due to cancellation of the upstream and downstream traveling waves.

The mechanical cutoff frequency of the microphone due to pressure equalization is about 5 Hz. Consequently below this frequency the cross spectrum shown in figure 11 is unreliable and the coherence shown in figure 13 is low.

Temperature Autospectra, Cross Spectra, and Coherence

A temperature-temperature constant-bandwidth (0.4 Hz) cross spectrum between the duct inlet and exit and temperature autospectra at the duct inlet and exit are shown in figures 14 and 15. These temperature measurements were made by using the thin thermocouples in the probes and are shown after correction for thermocouple response. At frequencies up to 120 Hz the phase angle of the cross spectrum changed linearly with frequency with a slope proportional to the time delay due to transport of temperature perturbations in the duct at the convective velocity. Based on the phase angle plot shown in figure 14, a 540° phase shift $\Delta\theta$ occurred over the first 18-Hz frequency interval Δf . Using the relation

$$v = \frac{360 \Delta f L}{\Delta\theta} \quad (15)$$

and taking the distance between measurement points L to be 5.44 m, the slope of the phase angle plot yields a velocity of 65 m/s. This is close to the measured velocity based on the mass flow rate, which is 66 m/s. The cross-spectrum magnitude rolls off 15 dB over the first 120 Hz and resembles the exit temperature autospectrum shown in figure 15(b). At frequencies above 120 Hz the magnitude is flat and the phase is random because the response of the thermocouples is reduced so much that the signals are at the level of the sys-

tem noise. In the corresponding uncompensated cross spectrum (not shown) the magnitude at 120 Hz is 40 dB down from its peak value.

The inlet-temperature autospectrum is flat, but the exit-temperature autospectrum rolls off 20 dB in the first 120 Hz. The exit-temperature autospectrum changes slopes at 120 Hz because the signal is at the level of the system noise above 120 Hz.

The temperature cross and autospectra have no peaks except for spikes at 60 and possibly 120 Hz caused by electrical power line noise. The convective temperature perturbation spectrum does not have any of the peaks present in the pressure cross spectra and autospectra shown in figures 11 and 12 because of axial standing waves.

The coherence function corresponding to the temperature cross spectrum in figure 14 is shown in figure 16. The shape of the coherence function does not correspond to the pressure autospectra or cross spectra. At frequencies greater than 120 Hz the coherence is very low because the signals are at the level of the system noise.

For liquid Jet A fuel, similar relationships between the duct inlet and exit temperature were found (ref. 6).

Pressure-Temperature Cross Spectra and Coherence

Duct inlet. - The pressure-temperature constant-bandwidth (0.8 Hz) cross spectrum at the duct inlet (station 3) is shown in figure 17. The magnitude plots of the pressure-temperature cross spectra resemble the magnitude plots of the corresponding inlet-pressure autospectra shown in figure 12(a). The phase angle variation in this region shows some evidence of a definite pattern, indicating a systematic relationship between pressure and temperature near the J-47 can combustor but not one clearly related to a convective time delay. Again, similar behavior was observed in the Jet A data (ref. 6).

The corresponding coherence function is shown in figure 18. A region of higher coherence appears between 80 and 240 Hz in figure 18 with peaks at frequencies corresponding to the largest pressure levels in the inlet pressure autospectrum (fig. 12(a)). Similar behavior was observed in the Jet A data (ref. 6).

Duct exit. - Pressure-temperature cross spectra and coherence functions are given for the thick thermocouple over frequency ranges from 0 to 160 Hz (figs. 19 and 20) and 0 to 320 Hz (figs. 21 and 22). The low-frequency range is shown because of the higher resolution it provides.

Examination of the low-frequency-range cross spectrum (fig. 19) shows the expected linear phase angle dependence due convection of temperature perturbations at the flow velocity.

Examination of the low-frequency-range coherence plot (fig. 20) shows that the thick-thermocouple signal is slightly more coherent with the pressure at high frequencies than at low frequencies. Below 60 Hz the coherence is large enough to provide some ordered phase angle information.

Examination of the high-frequency-range cross spectrum (fig. 21) shows that the peaks in the thermocouple magnitude plot resemble those in the corresponding pressure autospectrum (fig. 12(b)). Furthermore the linear phase angle dependence due to the convective temperature-time delay effect is again present. However, it is most clearly seen not at low frequencies but at high frequencies over several 10-Hz segments of the frequency axis near the peaks in the pressure autospectrum.

The pressure-temperature cross spectrum phase angle plot does clearly show segments having linear dependence with slopes that are proportional to the convected time delay that was observed in the Jet A fuel combustion data discussed in reference 6. However, the coherence at low frequencies was larger for the Jet A data.

At the exit, over the 0- to 320-Hz frequency range studied, it was observed that the duct exit phase angle of the pressure is related to the phase angle of the temperature by the convective time delay. Note that, since both measurements are made at the same point, the time delay is not related to a convective time delay between points. Rather, as in reference 6, the phase angle lag is essentially due to the time delay resulting from the difference in travel times of pressure and temperature signals from a point where the phase angle relationship between pressure and temperature does not change much.

The slope of the linear phase angle relationship is 22.25 deg/Hz near 220 Hz. By using the flow velocity (66 m/s), the relationship shown in equation (15), and this slope, the point at which the linear phase angle relationship is established was calculated to be 2.05 m from the duct inlet. Thus at distances further than 2.05 m from the duct inlet the phase angle relationship between pressure and temperature no longer changes much. Removal of this linear trend yields a phase angle plot similar to the one shown in figure 17 measured at station 3, located 0.7 m from the duct inlet. Since the linear relationship does not hold closer than 2.05 m from the duct inlet, we concluded that the phase angle relationship at station 3, near the duct inlet, is not consistent with a simple source model that assumes pressure and temperature are in phase at the source in the combustor and related to one another only by a convective time delay at all other locations downstream of the source. Thus these test results indicate that a more complex model of the source is required.

CONCLUSIONS

Based on the fluctuating pressure and temperature measurements made in the hydrogen-fueled combustion system and previous tests made with Jet A the following conclusions were reached for both fuels:

- (1) At the duct exit perturbations in pressure and temperature are related by the convective time delay.
- (2) Perturbations in temperature at the duct inlet and exit are related by the convective time delay.

(3) At the duct inlet perturbations in pressure and temperature show some evidence of a definite relationship, indicating an unknown but systematic relationship between pressure and temperature in the combustion region in addition to that due to the convection of temperature disturbances.

(4) At the duct inlet and exit the magnitudes of the cross spectra between pressure and temperature resemble the magnitudes of the corresponding pressure autospectra.

However, the significant coherence at low frequencies between the pressure and temperature at the duct exit observed in the Jet A data is not present.

The phase angle relationship between pressure and temperature at the duct inlet is not consistent with a simple source region model that assumes that pressure and temperature are in phase at the source point in the combustor and related to one another at downstream points by only a time delay due to convection of temperature disturbances. These test results that indicate a more complex model of the source region is required.

REFERENCES

1. J. H. Miles and E. A. Krejsa, "Pressure transfer function of JT15D nozzle due to acoustic and convected entropy fluctuations," J. Acoust. Soc. Am 72, 2008-2019 (1982).
2. R. R. Dils, "Dynamic gas temperature measurements in a gas turbine transition duct exit," J. Eng. Power 95, 265-277 (1973).
3. M. Muthukrishnan, W. C. Strahle, and D. H. Neale, "Separation of hydrodynamic, entropy, and combustion noise in a gas turbine combustor," AIAA J. 16, 320-327 (1978).
4. T. G. Sofrin and N. Riloff, Jr., "Experimental Clean Combustor program - noise study," PWA-5458, Pratt & Whitney Aircraft, East Hartford, Conn., NASA CR-135106 (September 1976).
5. D. C. Mathews, N. F. Rekos, Jr., and I. Nagel, "Combustion noise investigation," FAA RD-77-3, PWA-5478, Pratt & Whitney Aircraft Group, East Hartford, Conn. (February 1977).
6. J. H. Miles, C. A. Wasserhauer, and E. A. Krejsa, "Cross spectra between temperature and pressure in a constant area duct downstream of a combustor," NASA TM-83351 (1983).
7. A. M. Karchmer and M. Reshotko, "Core noise source diagnostics on a turbofan engine using correlation and coherence techniques," NASA TM X-73535 (1976).
8. A. M. Karchmer, M. Reshotko, and F. J. Montegani, "Measurement of far field combustion noise from a turbofan engine using coherence functions," AIAA Paper 77-1277 (October 1977).
9. W. C. Strahle and M. Muthukrishnan, "Thermocouple time constant measurement by cross power spectra," AIAA J. 14, 1642-1644 (1976).
10. A. J. Yule, D. S. Taylor, and N. A. Chigier, "Thermocouple signal processing and on-line digital compensation," J. Energy 2, 223-231 (1978).
11. M. J. D. Powell, "An efficient method for finding the minimum of a function of several variables without calculating derivatives," Comput. J., 7, 155-162 (1964).
12. M. S. Shapiro and M. Golubstein, A collection of mathematical computer routines, (New York University, New York, 1965), NYO-1480-14.

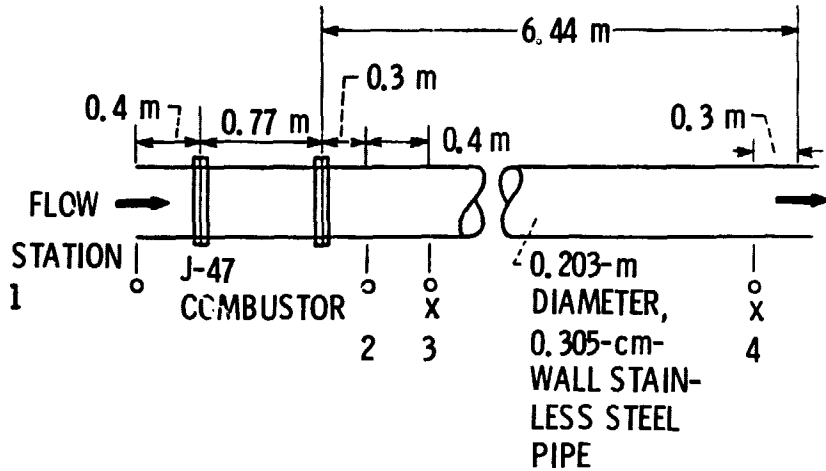
TABLE I. - TEST CONDITIONS AND THERMOCOUPLE TIME CONSTANTS

[Test conditions: inlet-temperature perturbation, T_{inlet} , 660 K; exit-temperature perturbation, T_{exit} , 765 K; air mass flow rate, W_{air} , 1.09 kg/s; mean flow velocity, V , 66 m/s.]

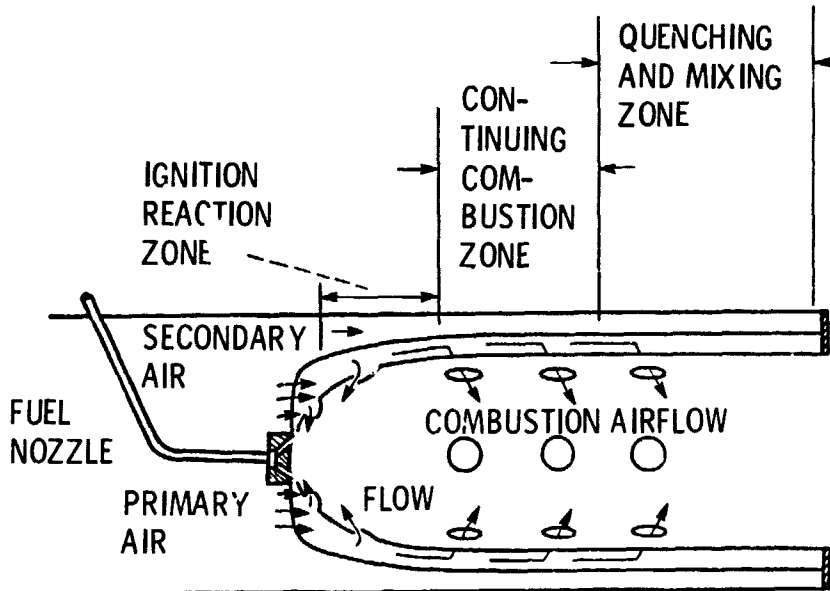
Thermocouple constant	Inlet (station 3)		Exit (station 4)	
	Thick	Thin	Thick	Thin
Diameter, d , μm	76.2	25.4	76.2	25.4
Thermocouple time constant, τ , ms	55.80	26.21	54.12	20.88
Thermocouple parameter, A	2.37	17.52	10.69	7.61
Bead thermocouple time constant, τ_b , ms	42.80	20.00	11.52	2.54

ORIGINAL PAGE IS
OF POOR QUALITY

- o INFINITE TUBE MICROPHONE
- x DUAL-THERMOCOUPLE PROBE



(a) RIG SCHEMATIC.



(b) INJECTION SCHEME.

Figure 1. - Schematic of ducted combustion system rig.

ORIGINAL PAGE IS
OF POOR QUALITY

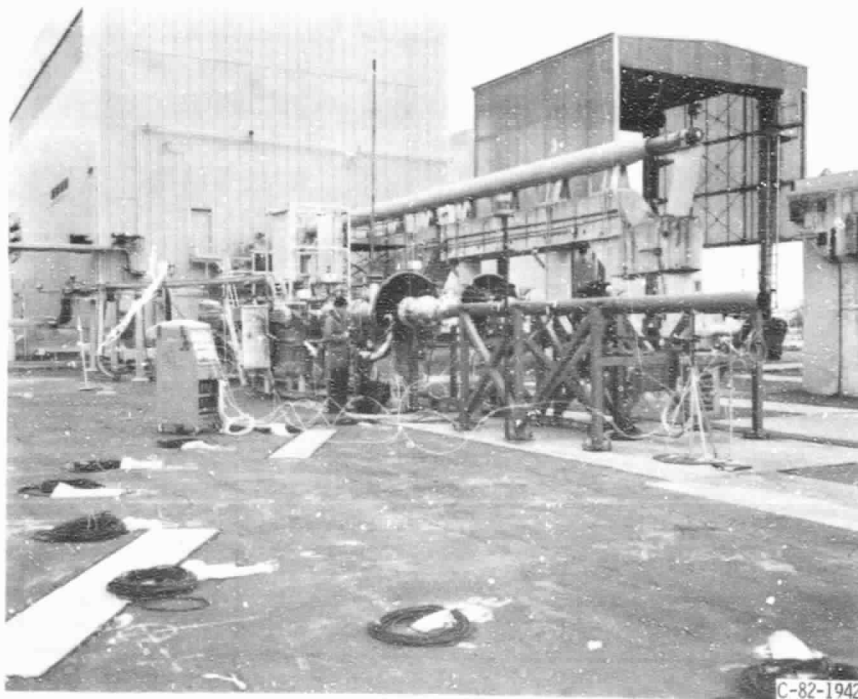


Figure 2. - NASA Lewis combustion acoustics facility.

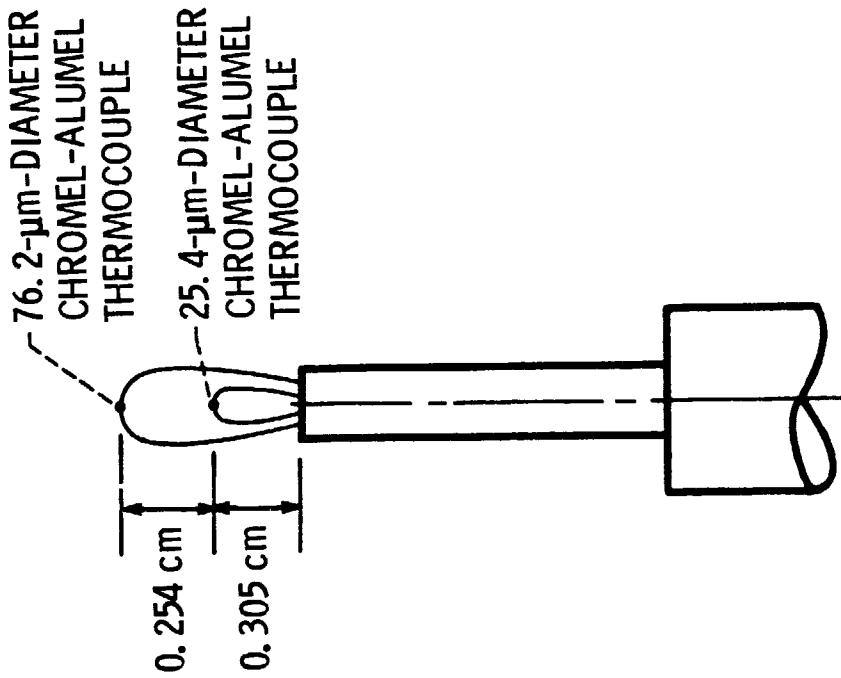


Figure 3. - Dual-thermocouple probe design.

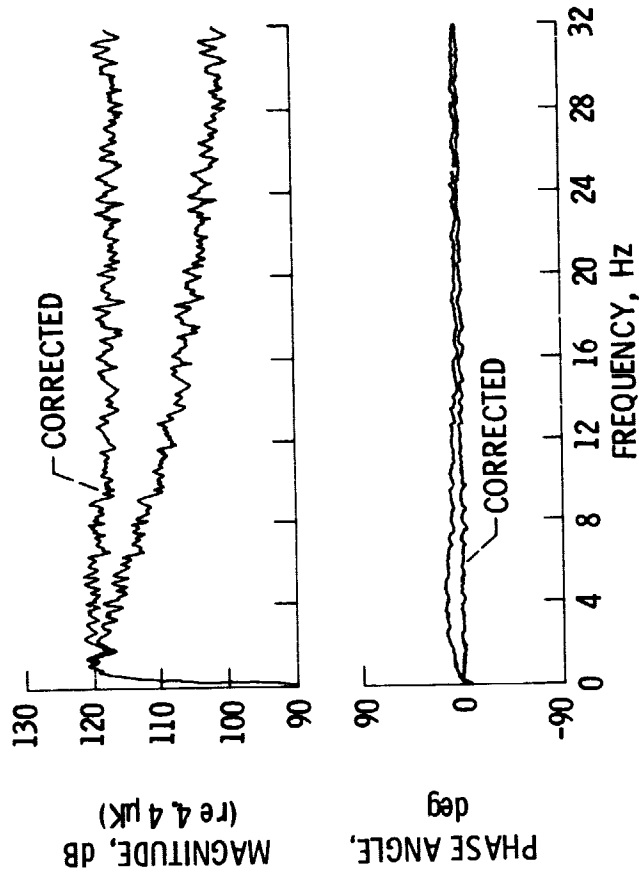
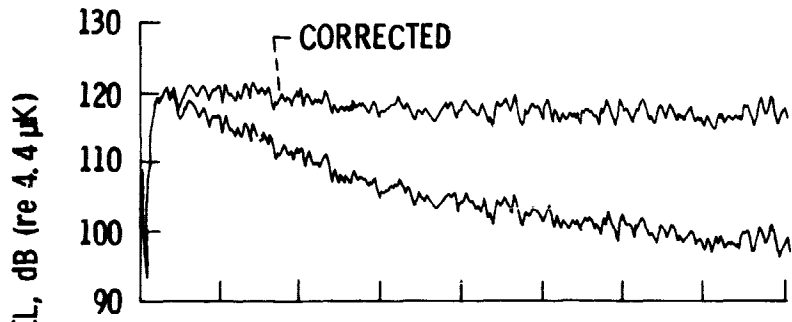
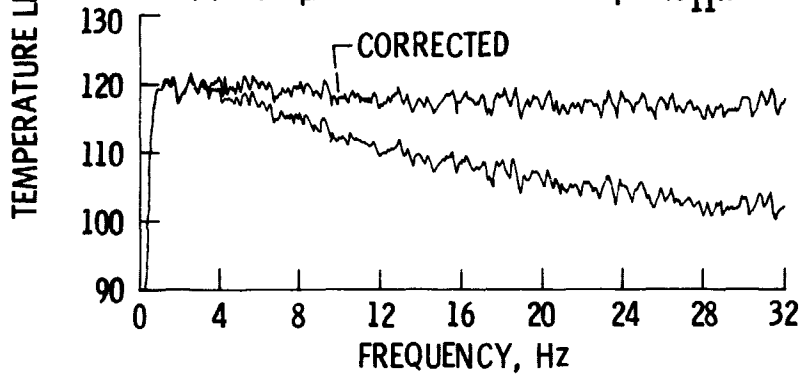


Figure 4. - Temperature cross spectrum between thick and thin thermocouples (G_{12}) at duct inlet (station 3) for bandwidth of 0.08 Hz.



(a) 76.2- μm -diameter thermocouple (G_{11}).



(b) 25.4- μm -diameter thermocouple (G_{22}).

Figure 5. - Temperature autospectra of thick and thin thermocouples at duct inlet (station 3) for bandwidth of 0.08 Hz.

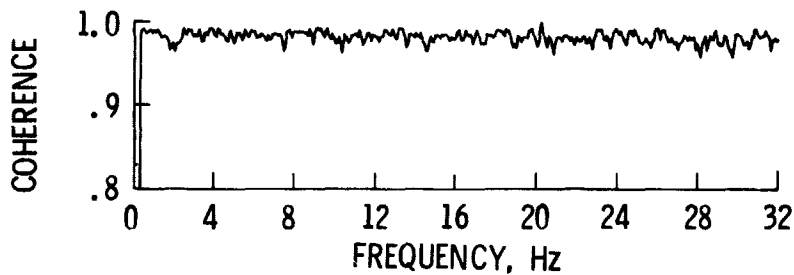


Figure 6. - Temperature coherence between thick and thin thermocouples at duct inlet (station 3) for bandwidth of 0.08 Hz.

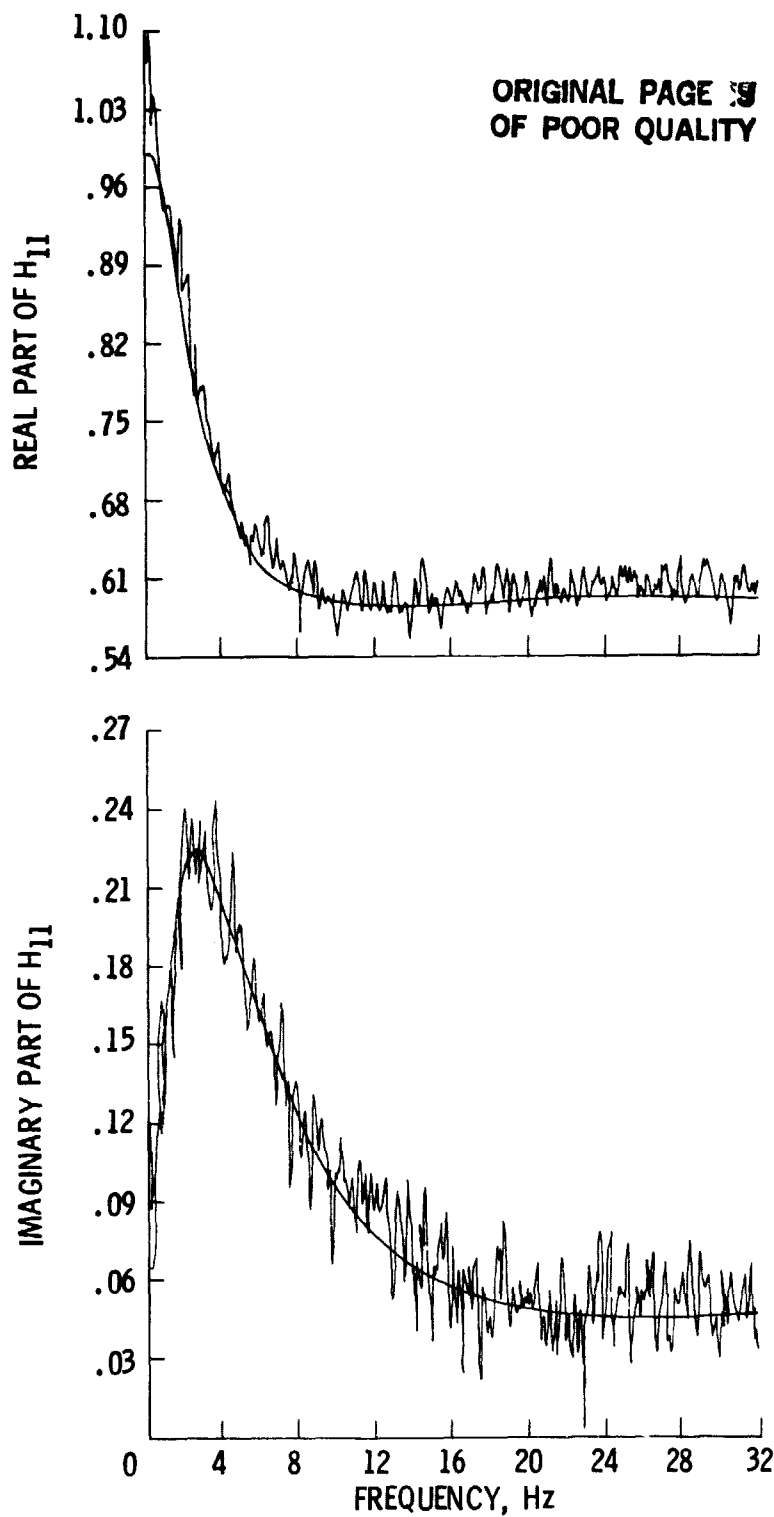


Figure 7. - Thick-thermocouple autospectra ratio ($H_{11} = G_{11}/G_{22}$) at duct inlet (station 3) for bandwidth of 0.08 Hz.

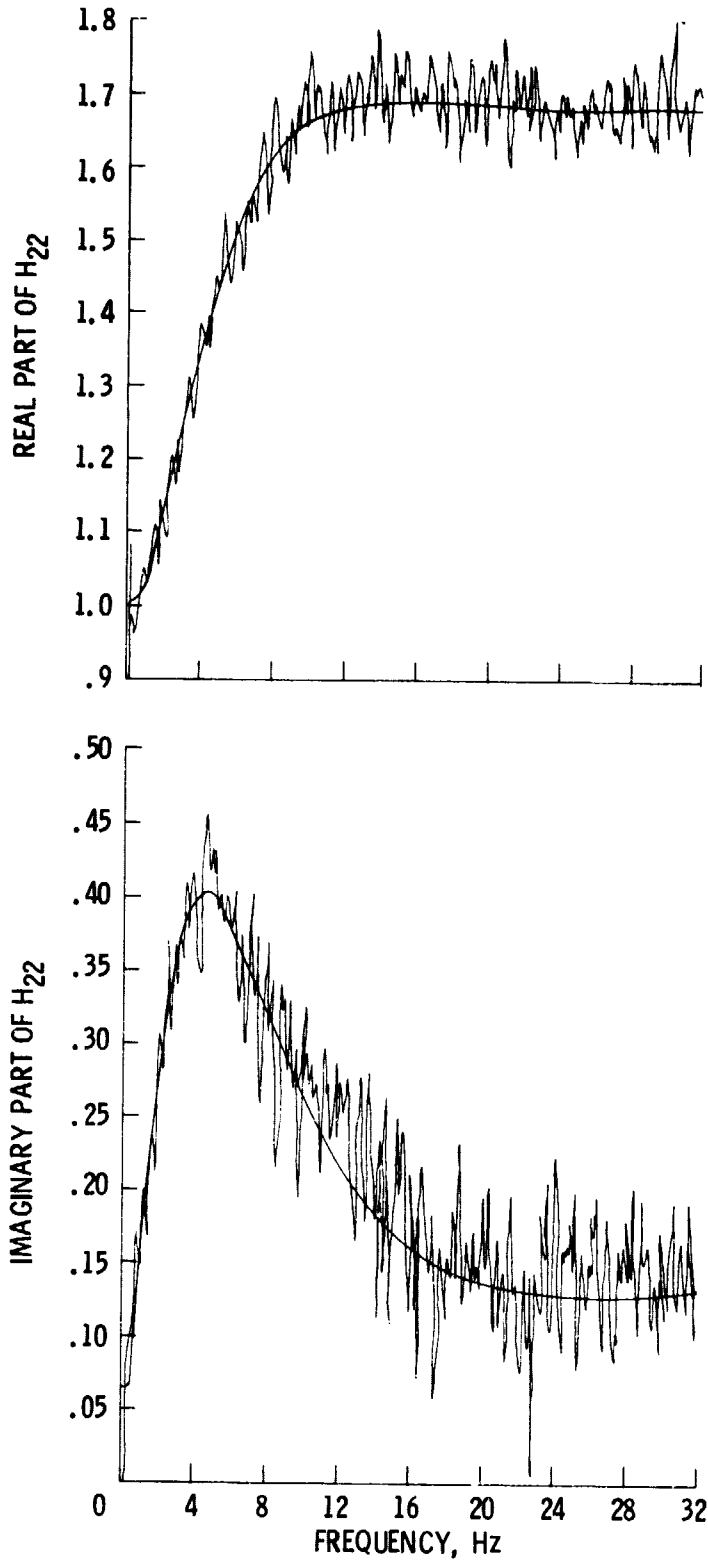


Figure 8. - Thin-thermocouple autospectra ratio
($H_{22} = G_{22}/G_{12}$) at duct inlet (station 3) for band-
width of 0.08 Hz.

ORIGINAL PAGE IS
OF POOR QUALITY

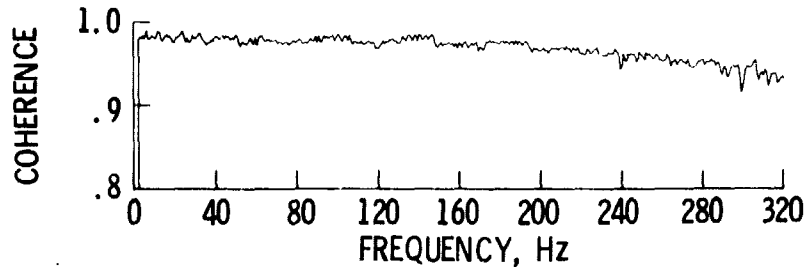


Figure 9. - Temperature coherence between thick and thin thermocouples at duct inlet (station 3) for bandwidth of 0.8 Hz.

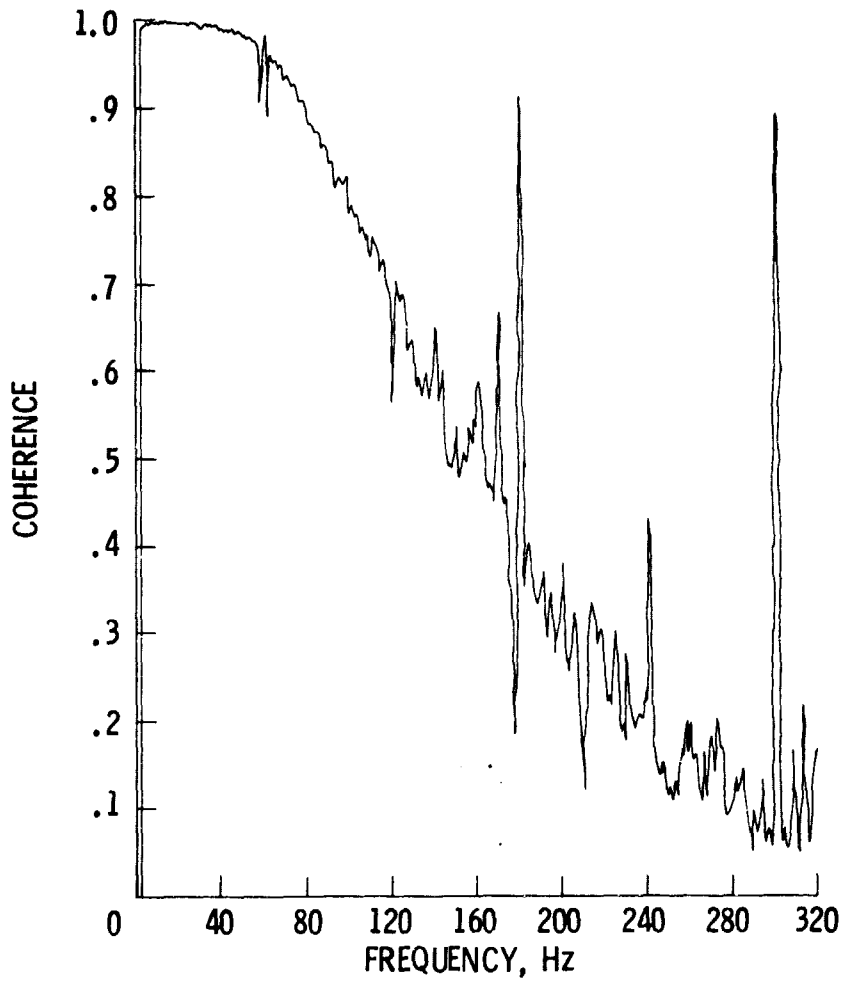


Figure 10. - Temperature coherence between thick and thin thermocouples at duct exit (station 4) for bandwidth of 0.8 Hz.

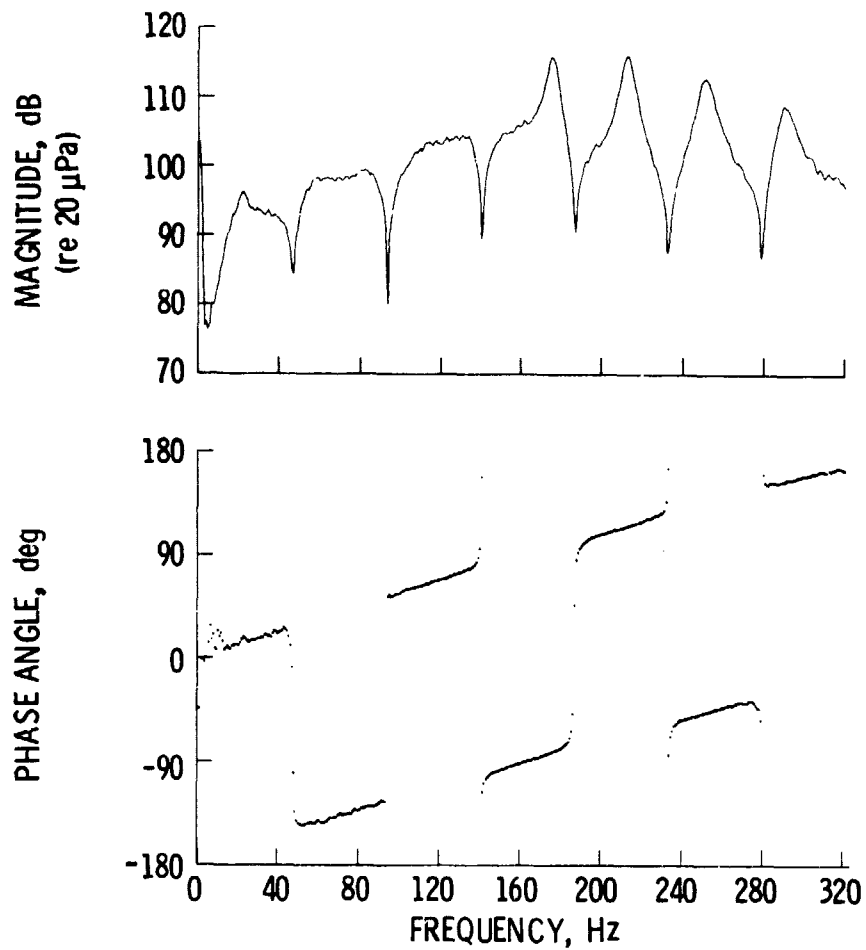


Figure 11. - Pressure cross spectra $p_4 p_3^*$ between duct inlet (station 3) and duct exit (station 4) for bandwidth of 0.8 Hz.

ORIGINAL PAGE IS
OF POOR QUALITY

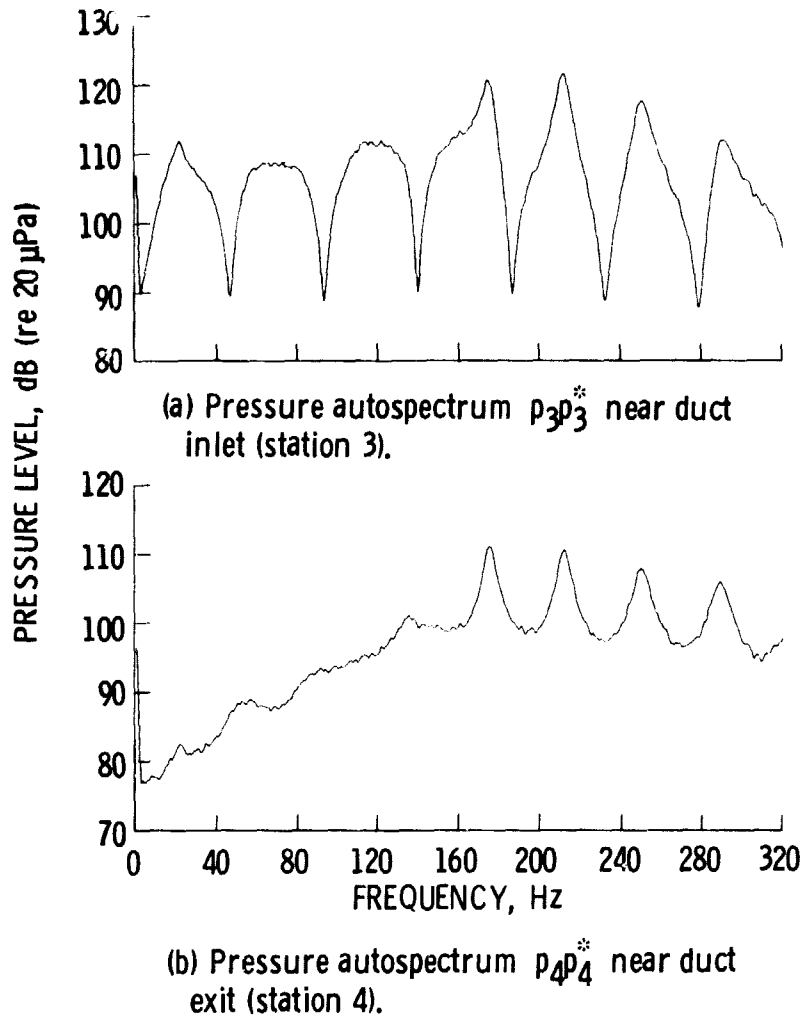


Figure 12. - Pressure autospectra for bandwidth of 0.8 Hz.

ORIGINAL FACE IS
OF POOR QUALITY

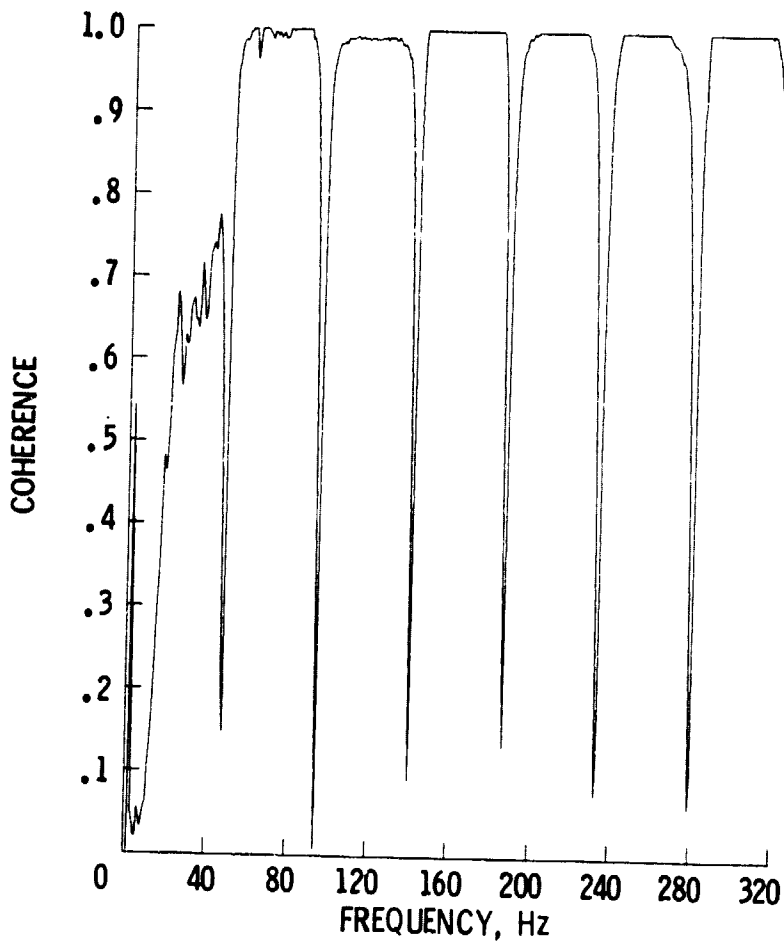


Figure 13. - Pressure coherence $|p_4 p_3^*|^2 / |p_4|^2 |p_3|^2$ between duct inlet (station 3) and duct exit (station 4) for bandwidth of 0.8 Hz.

ORIGINAL PAGE IS
OF POOR QUALITY

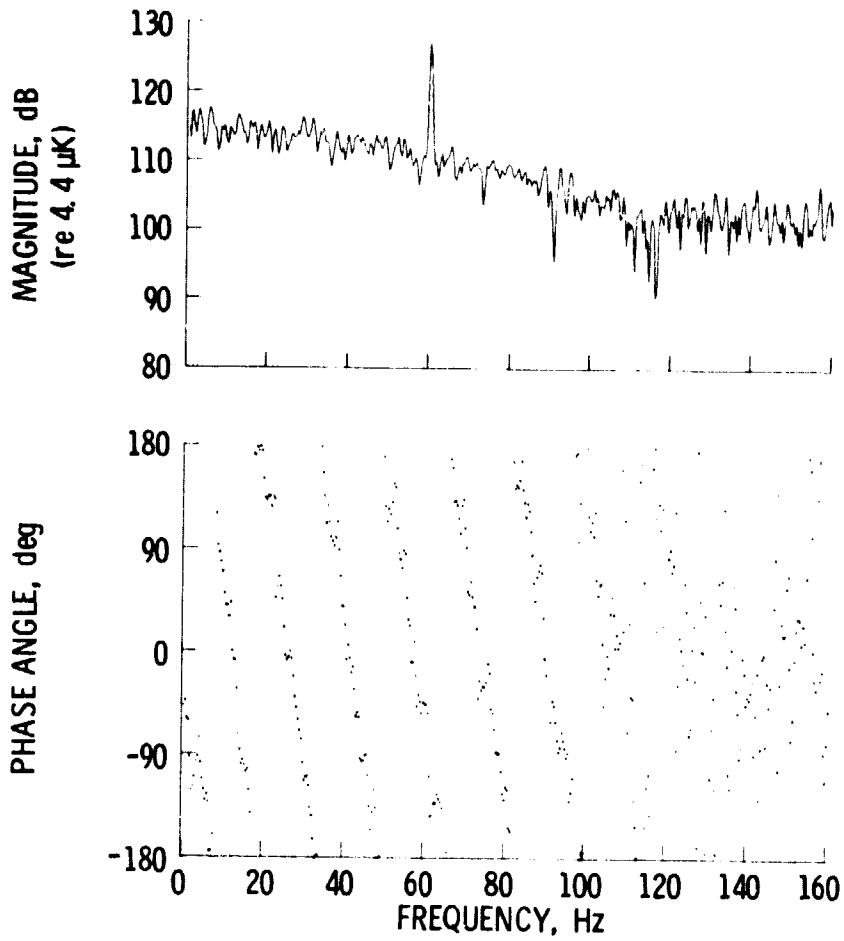


Figure 14 - Temperature cross spectra $T_4 T_3^*$
between duct inlet (station 3) and duct exit
(station 4) for bandwidth of 0.8 Hz.

ORIGINAL PAGE IS
OF POOR QUALITY

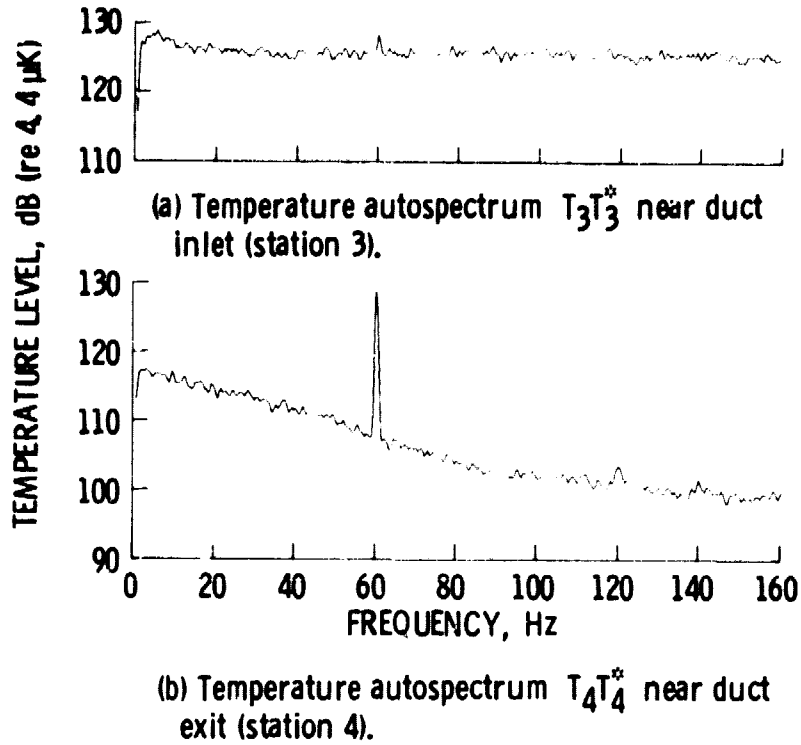


Figure 15. - Temperature autospectra for bandwidth of 0.8 Hz.

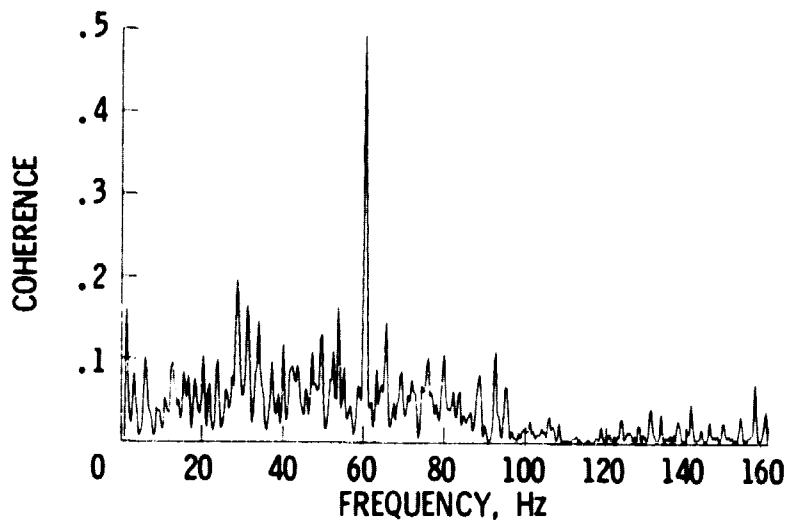


Figure 16. - Temperature coherence $|T_4T_3^*|^2 / |T_4|^2 |T_3|^2$ between duct inlet (station 3) and duct exit (station 4) for bandwidth of 0.4 Hz.

ORIGINAL PAGE IS
OF POOR QUALITY

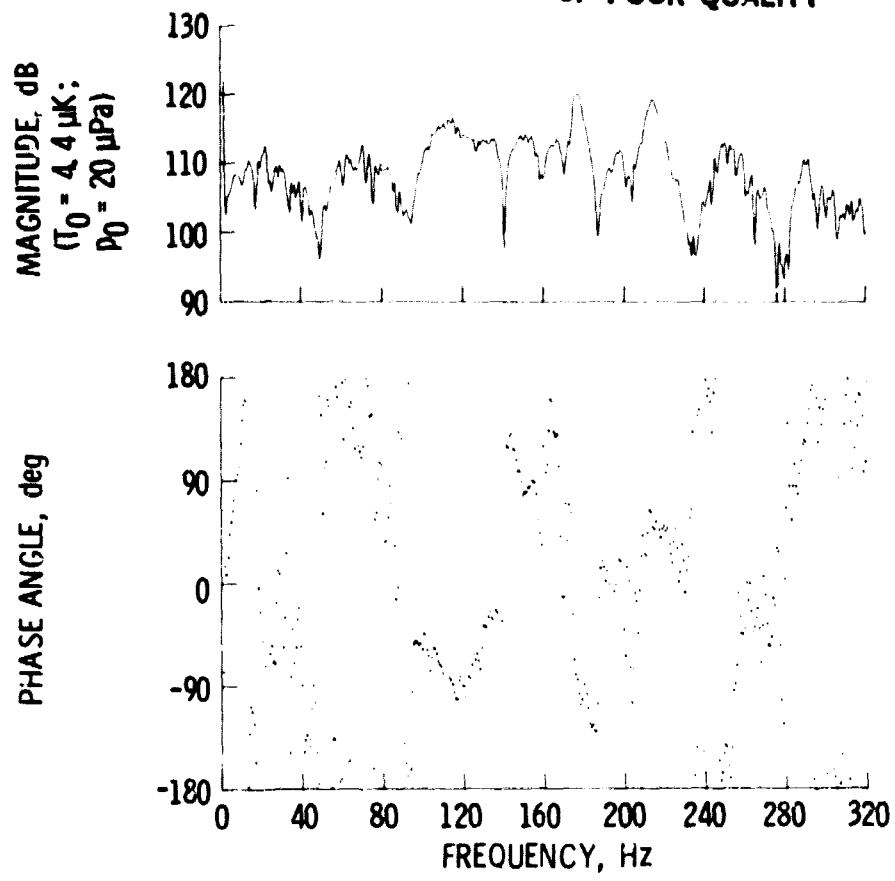


Figure 17. - Cross spectra between pressure and temperature $p_3 T_3^*$ at duct inlet (station 3) for bandwidth of 0.8 Hz.

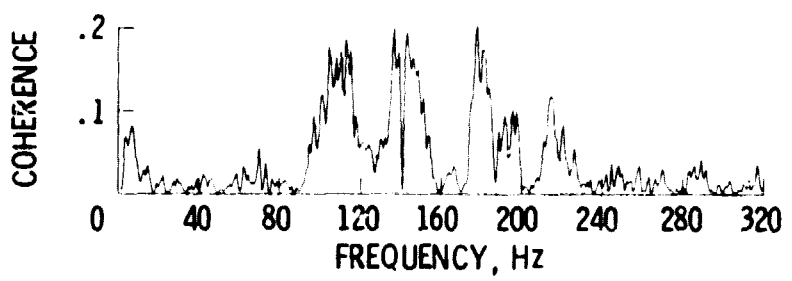


Figure 18. - Coherence between pressure and temperature $|p_3 T_3^*|^2 / |p_3|^2 |T_3|^2$ at duct inlet (station 3) for bandwidth of 0.8 Hz.

ORIGINAL PAGE IS
OF POOR QUALITY

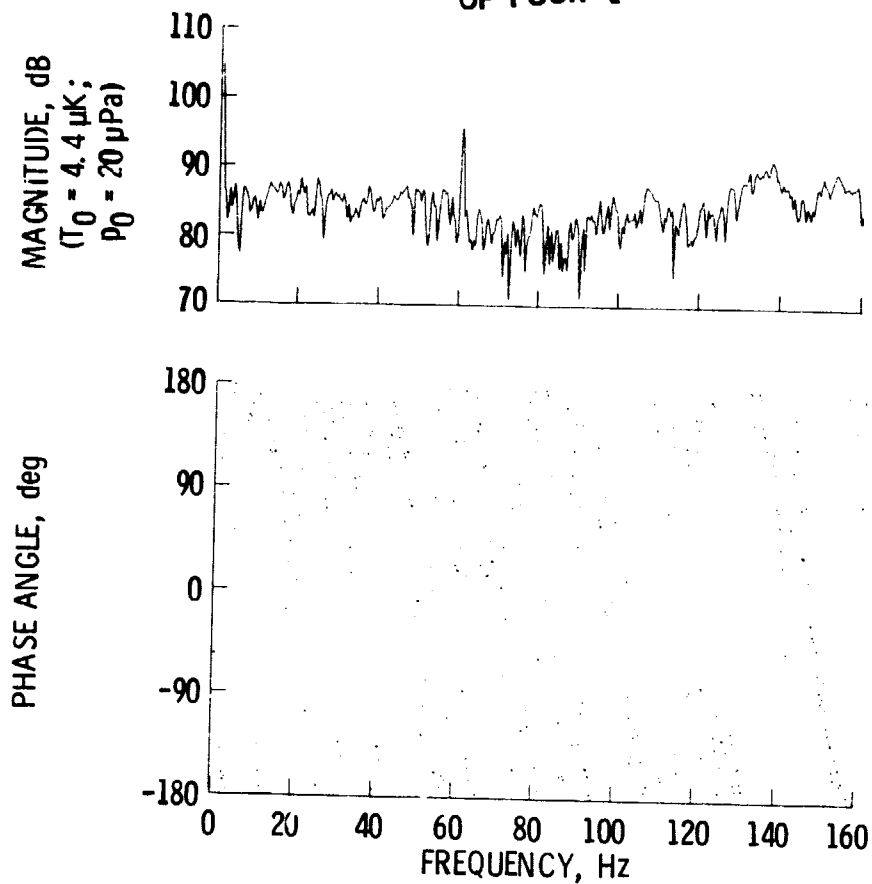


Figure 19. - Cross spectra between pressure and temperature $p_4 T_4^*$ at duct exit (station 4) for thick thermocouple and bandwidth of 0.4 Hz.

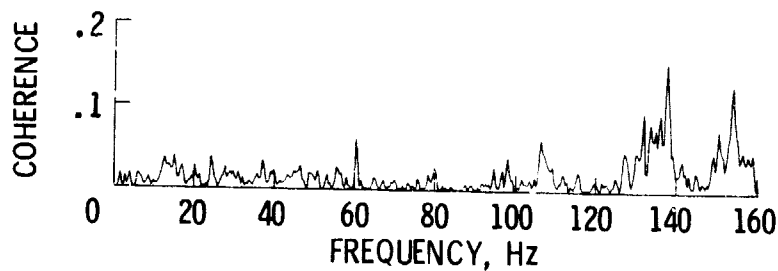


Figure 20. - Coherence between pressure and temperature $|p_4 T_4^*|^2 / |p_4|^2 |T_4|^2$ at duct exit (station 4) for thick thermocouple and bandwidth of 0.4 Hz.

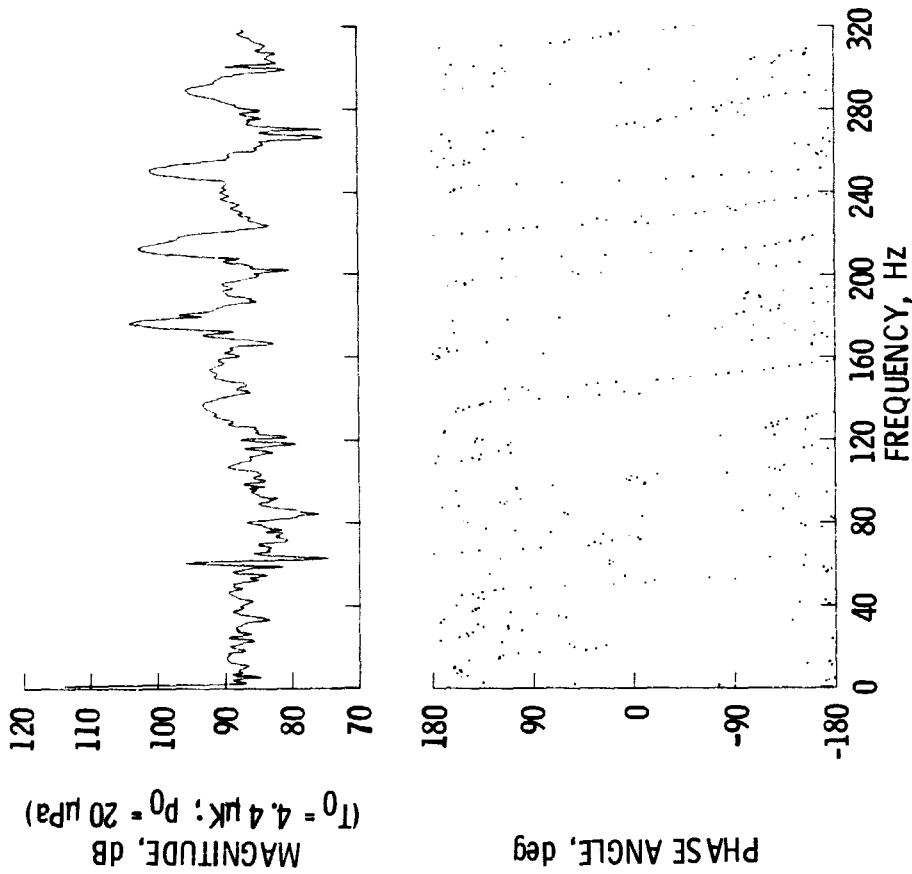


Figure 21. - Cross spectra between pressure and temperature p_{T4} at duct exit (station 4) for thick thermocouple and bandwidth of 0.8 Hz.

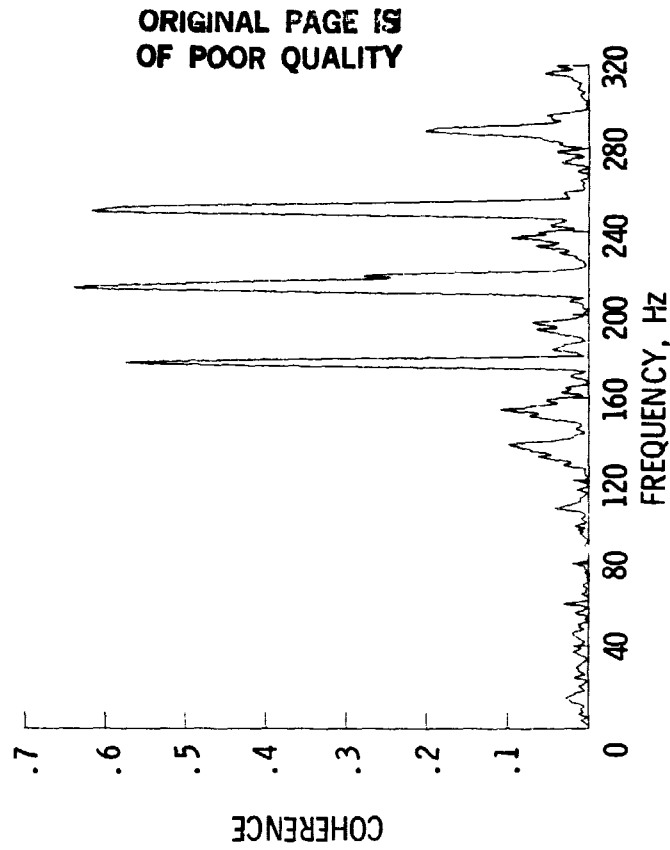


Figure 22. - Coherence between pressure and temperature p_{T4} at duct exit (station 4) for thick thermocouple and bandwidth of 0.8 Hz.

ORIGINAL PAGE IS
OF POOR QUALITY